Chaos, Solitons and Fractals 174 (2023) 113782

Contents lists available at ScienceDirect

Chaos, Solitons and Fractals

journal homepage: www.elsevier.com/locate/chaos

Oscillations in SIR behavioural epidemic models: The interplay between behaviour and overexposure to infection

Bruno Buonomo [a,*], Andrea Giacobbe [b]

[a] Department of Mathematics and Applications, University of Naples Federico II, via Cintia, I-80126 Naples, Italy
[b] Department of Mathematics and Informatics, University of Catania, Viale A. Doria 6, I-95125 Catania, Italy

ARTICLE INFO

Keywords:
Social distancing
Overexposure
Human behaviour
Memory effects
Oscillations

ABSTRACT

Oscillations in epidemic models including human behaviour indicate that the human factor might play a key role in the occurrence of periodically high levels of incidence and prevalence of the disease. Such phenomena can be captured even with minimal models, i.e. basic SIR or SEIR models with a reduced mathematical complexity. In such models, the effects of information-dependent changes in contact patterns are strongly affected by the function used to describe the memory of the population. In particular, the endemic equilibrium cannot be destabilized in case of exponentially fading memory but sustained oscillations are possible when the memory of the population is described by certain unimodal functions. In this work, we introduce a behavioural SIR-like model with information-dependent social distancing to investigate the interplay between individuals' behaviour and overexposure to infection due to unconscious exposure to contagion. We use spectral analysis to show that sustained oscillations may take place even with exponentially fading memory. We show that this result holds both in case of prevalence-based and incidence-based social distancing. Furthermore, we show that the individual's behavioural response to information may stabilize the oscillations induced by overexposure.

1. Introduction

Mathematical models for the dynamics of infectious diseases have proved to be useful in helping policy makers to plan surveillance and community-based control of epidemics, even during the current coronavirus pandemic [1–4]. Among the *epidemic models*, a major role is played by the *compartmental models*, where the population affected by an infectious disease is divided into mutually exclusive groups according to their status with respect to the disease [5,6]. Epidemics may be described by a single compartmental model [2,3,7] or compartmental models may be part of network models [8–10]. The construction of compartmental models is based on several specific assumptions that must correctly represent the problem under examination. These include two important issues: the first is how to choose the function that must represent the *force of infection* (FoI), i.e. the per capita rate at which susceptibles get infected. The second issue arises from the observation that in many cases the individuals change their behaviours according to the development of the epidemic; that is, the individuals adapt their contacts at risk, make vaccine-related decisions, enter voluntary quarantine, and so on, according to the current and the past status of the disease in the community where they live. This, in turn, produces a feedback on the course of the outbreak [11,12]. Therefore, the second issue is how the individuals' response to the epidemic must be taken into account when designing an epidemic model.

In 1978, both these issues where addressed by V. Capasso and G. Serio in their well known study on the generalization of the Kermack-McKendrick epidemic model [13]. They proposed that the FoI should depend on the *prevalence* (i.e. the size of infectious in the population) and should describe the following circumstance: when the perceived risk of infection become very large, the individuals enhance self-protection measures so that the risk of getting the disease reduces. Therefore, it is required that the FoI saturates (i.e. grows monotonically to a given finite value) or is a non-monotone function that increases till a peak and then decreases to zero. Epidemic models including nonlinear FoI are also called *behaviour-implicit models* [14] and have been extensively used in the Mathematical Epidemiology literature [6,15].

In the last few years, behaviour-implicit models have been generalized to behaviour-*explicit* models, where the FoI depends on the current and past values of prevalence through the so-called *information index* [11,12]. Such an index is a distributed delay containing a memory kernel. When the memory kernel is a Dirac's delta function (which represents the case where the public gets instantaneous information on the current prevalence), one finds the phenomenological model proposed by Capasso and Serio (see [14] for more details).

* Corresponding author.
E-mail addresses: buonomo@unina.it (B. Buonomo), giacobbe@dmi.unict.it (A. Giacobbe).

https://doi.org/10.1016/j.chaos.2023.113782
Received 4 May 2023; Accepted 3 July 2023
Available online 19 July 2023

Models that explicitly includes information-induced behavioural changes constitute nowadays a well established tool of *Behavioural Epidemiology of Infectious Diseases* (see e.g. the recent papers [7,16–18]). Such models often show new outcomes, when compared with non-behavioural models [11,12]. Besides of the theoretical studies, the behaviour-explicit models have been applied to the case of COVID-19 where an estimate of the information-related parameters has been obtained by employing official data released by the public health system [7].

A case of special interest in behavioural modelling is when the individuals adjust their social contacts according to the available information and rumours about the status of the disease in the community where they live [19]. This scenario, for instance, may be considered to study the phenomenon of non compliance to mitigation measures like, e.g., the social distancing [16,20]. In 2009, d'Onofrio and co-workers proposed to study this problem through a SIR model with demography and information-dependent contact rate [19]. They showed that when the memory of the population is exponentially fading (i.e. the memory kernel included in the information index is a *weak* Erlangian kernel) the model outcome is similar to that of the classical SIR model: the disease will disappear or approach an endemic steady state according to if the basic reproduction number R_0 is, respectively, below or above the critical value $R_0 = 1$. However, when the current information is unavailable and the information arrives to the public after a given average time delay (i.e. the memory kernel included in the information index is an unimodal *strong* Erlangian kernel), then sustained oscillations are possible when $R_0 > 1$. This interesting feature not only holds when the behavioural responses of individuals is linked to *prevalence*, as considered in [19], but also when the behavioural responses are based on the available information on the *incidence* (i.e. the new cases during a particular time period) [16].

We remark that detecting oscillations in epidemic models is very important since oscillations lead to periodically high level of incidence and prevalence that can be dangerous for the population. Moreover, oscillations inherent in epidemic models may resonate with periodic forcing (like seasonality) resulting in an anomalous prevalence rise. Detecting oscillations in *behavioural* models is particularly relevant, since it indicates that the human behaviour might be a fundamental factor when oscillations in time-series of endemic diseases are observed [12]. Therefore, the analysis of the effects of the interplay between human behaviour and other nonlinearities included in epidemic models goes beyond the theoretical investigation and has interesting practical aspects.

A specific form of the FoI that has attracted the interest of many authors is given by the following convex functional [21]:

$$\text{FoI} = \beta \left(I + \alpha I^2 \right), \tag{1}$$

where I denotes a measure of the prevalence, the positive constant β denotes the transmission rate (which includes the contact rate) and α is a positive constant (sometimes called *overexposure coefficient* [22]). The convex formulation of the FoI is not typical in epidemic models with nonlinear FoI where, as mentioned above, the FoI is commonly described by a saturating function or a non monotone function that asymptotically approaches zero. In (1) the term βI is usually described as the force of infection produced by single contacts whereas $\beta\alpha I^2$ is an additional term due to two exposures over a short time period [21]. Interestingly, the functional (1) has been used to represent the *overexposure* produced by unconscious exposure to contagion to which a susceptible is subject in presence of asymptomatic infectious individuals [23]. This idea has been applied to the case of COVID-19 disease [22].

It is worth mentioning that a similar modelling approach has been used also to represent the influence of *peer-pressure* [24] in the spread of 'social diseases' like health risky behaviours (smoking, heavy drinking or drug abuse) [25,26].

Epidemic models where the FoI is described by (1) show special dynamical features that are not usual in models with 'classical' FoI like Hopf and Bogdanov–Takens bifurcations [27], catastrophic collapse of the basin of attraction for the endemic state associated with the existence of homoclinic orbits [28], hysteresis through backward transcritical bifurcations [21,22,28].

Motivated by the above considerations, in this paper we introduce a minimal SIR-like behavioural model to investigate the interplay between individuals' behavioural response and overexposure to infection. We will use spectral analysis to assess the effects produced by information-dependent social distancing in both the case of prevalence-based and incidence-based social distancing.

The rest of the paper is organized as follows: In Section 2 we will recall basic topics of behavioural modelling and will introduce the SIR-like model with prevalence-based social distancing and overexposure. In Section 3 we present some preliminary qualitative analysis, including rescaling, positive invariance and the existence of equilibria. In Section 4 we discuss the stability of the equilibria through spectral analysis and provide numerical simulations. The case of incidence-based social distancing is discussed in Section 5. Conclusions are given in Section 6.

2. The prevalence-based SIM model with overexposure

We consider the following epidemic model with a convex FoI representing the overexposure:

$$\begin{aligned} \dot{S} &= \mu (1 - S) - f(M) S I (1 + \alpha I) \\ \dot{I} &= f(M) S I (1 + \alpha I) - (\mu + \gamma) I, \end{aligned} \tag{2}$$

where S and I denote, respectively, the fractions of susceptible and infectious individuals within a given population. All the parameters in (2) are positive constants: μ is the birth rate, which is assumed to be identical to the natural death rate; γ is the recovery rate from the disease and α is the overexposure parameter.

When $\alpha = 0$, model (2) reduces to the behavioural SIR-M model introduced in 2009 by d'Onofrio and Manfredi [19].

The population includes also recovered individuals, whose fraction is denoted by R and satisfies $\dot{R} = \gamma I - \mu R$. Therefore the total population is constant and $R = 1 - S - I$.

Model (2) is a *behavioural* epidemic model because it takes into account the fact that the individuals may alter the contact rate among themselves (and, in turn, the transmission rate of the disease) by adopting social distancing. The choice to adhere to social distancing is assumed to be on voluntary basis and influenced by the circulating information and rumours about the disease spread. From a mathematical point of view, this input is represented by the quantity $M(t)$, called *information index* [11,12]. Generally speaking, the information index is given by the following distributed delay:

$$M(t) = \int_{-\infty}^{t} g(\tau) K(t - \tau) d\tau, \tag{3}$$

where K is the *memory kernel* and g the *message function*. As we will discuss below, the message function must be chosen appropriately to describe the kind of information that the individuals consider to be relevant in determining their final choice to adopt or not to adopt social distancing.

Before giving the specific forms of K and g, we discuss the function $f(M)$ in (2), which describes the effects of the information and rumours on the transmission rate. We assume that higher levels of awareness induced by information and rumours leads to a lower transmission rate. Therefore $f(M)$ is assumed to be a sufficiently regular function such that $f(0) = \beta$ (the *baseline* transmission rate in absence of behavioural response), $f(M) > 0$ and $f'(M) < 0$, for every $M \geq 0$. A function satisfying those requisites, already used for SIM models [19], is the following:

$$f(M) = \frac{\beta}{1 + \zeta M}, \tag{4}$$

where the positive constant parameter ζ is the *reactivity factor* of voluntary change in contact patterns: for a given level of information M, the greater this factor is, the lower is the contact rate. In other terms, the parameter ζ represents the influence of social distancing on the transmission rate.

Going back to (3), we say that the social distancing is *prevalence-based* when the message function g depends only on the prevalence I. The simplest type of dependence is linear, and g is proportional to I [12,19]:

$$g_{prev}(\tau) = k\, I(\tau). \tag{5}$$

In Section 5, we will discuss the case of *incidence-based* social distancing, when the message function g depends on the incidence of the disease. The simplest type of dependence is when g is proportional to the term $f(M)SI(1+\alpha I)$ in (2).

When (5) is adopted, the constant parameter k is called *information coverage*. It is assumed to be positive and $k \le 1$ to mimic possible under-reporting due to imperfect procedures, lack of media appeal or actions aimed at avoiding extreme social alarm [29].

As for the memory kernel K, a good compromise between realism and mathematical tractability is the Erlang distribution:

$$K(x) = Er_{n,\varepsilon}(x) = \frac{\varepsilon^n}{(n-1)!} x^{n-1} e^{-\varepsilon x};$$

where $x \in \mathbb{R}^+$, $n \in \mathbb{N}^+$ (*shape parameter*) and $\varepsilon \in \mathbb{R}^+$ (*rate parameter*).

An Erlangian kernel has the advantage of making the corresponding integro-differential system reducible into ordinary differential equations through the so-called *linear chain trick* [30].

Since

$$Er'_{1,\varepsilon} = -\varepsilon Er_{1,\varepsilon}, \qquad Er'_{n,\varepsilon} = \varepsilon(Er_{n-1,\varepsilon} - Er_{n,\varepsilon}), \qquad n > 1,$$

one obtains that, defining $M_j(t) = \int_{-\infty}^{t} g(\tau) Er_{j,\varepsilon}(t-\tau)d\tau$, the following additional equations must be added to model (2):

$$\begin{aligned} &\dot{M}_1 = \varepsilon\left(g - M_1\right) \\ &\cdots \\ &\dot{M}_n = \varepsilon\left(M_{n-1} - M_n\right). \end{aligned} \tag{6}$$

Even if a large part of the results that we obtain holds for systems with general Erlangian, here we consider only the case of a first order Erlang memory kernel $Erl_{1,\varepsilon}(\cdot)$ (also said *weak Erlangian kernel*), i.e. the case of *exponentially fading memory*, where the memory is distributed around the mean $T = 1/\varepsilon$. In this case the characteristic parameter ε may be interpreted as the inverse of the average time necessary to collect the information about the disease prevalence.

We conclude this section by collecting together ((2), (3), (4), (5)). The prevalence-based SIM model with overexposure can be written:

$$\begin{aligned} \dot{S} &= \mu(1-S) - \frac{\beta}{1+\zeta M} SI(1+\alpha I) \\ \dot{I} &= \frac{\beta}{1+\zeta M} SI(1+\alpha I) - \nu I \\ \dot{M} &= \varepsilon(kI - M), \end{aligned} \tag{7}$$

where we have set $\nu = \mu + \gamma$.

We remark again that when $\alpha = 0$ the model reduces to the SIM model considered by d'Onofrio and Manfredi [19]. In such a case, they proved that a first order Erlang memory kernel is *unable* to produce oscillations while sustained oscillations are possible when a second order Erlang memory kernel (also said *strong Erlangian kernel*) is considered.

Finally, when $\zeta = 0$, i.e. when the behavioural response is not taken into account, the model is similar to the SIS model considered by van den Driessche and Watmough [21] as well as to the SIRS model considered by Jin et al. [27].

3. Rescaling and equilibria

In order to reduce the number of independent parameters, we make a linear change in the variables. By rescaling time with $\tau = \varepsilon t$, and posing

$$X = S, \quad Y = \frac{\nu}{\mu} I, \quad Z = \frac{\nu}{k\mu} M, \quad a = \frac{\mu}{\nu}\alpha,$$

$$b = \frac{1}{\nu}\beta, \quad c = \frac{\mu k}{\nu}\zeta, \quad m = \frac{1}{\epsilon}\mu, \quad n = \frac{1}{\epsilon}\nu,$$

system (7) can be recast in the form

$$\begin{aligned} X' &= m\left(1 - X - b\frac{1+aY}{1+cZ} XY\right) \\ Y' &= n\left(-Y + b\frac{1+aY}{1+cZ} XY\right) \\ Z' &= Y - Z. \end{aligned} \tag{8}$$

In these equations we used a prime to denote the derivative with respect to τ (a dot denotes the derivative with respect to t). The number of nondimensional parameters is hence reduced to five. The parameters m, n are directly connected to the exit rates (mortality and recovery), a is linked to overexposure and c to the behavioural response of individuals. As we will see later on, b will be the basic reproduction number. The solution of system (8) are positive and bounded (see Appendix).

We now look for equilibria $E = (\tilde{X}, \tilde{Y}, \tilde{Z})$ of system (8). From the third equation of (8) one gets $\tilde{Z} = \tilde{Y}$. Hence from the second equation one has that either $\tilde{Y} = 0$, which gives the *disease-free* equilibrium $DFE = (1, 0, 0)$, or

$$\tilde{X} = \frac{1 + c\tilde{Y}}{b(1 + a\tilde{Y})}. \tag{9}$$

Substituting this quantity in the first equation one obtains:

$$ab\tilde{Y}^2 + (b + c - ab)\tilde{Y} + (1 - b) = 0. \tag{10}$$

It follows that there can possibly be two endemic equilibria, $E_+ = (X_+, Y_+, Z_+)$ and $E_- = (X_-, Y_-, Z_-)$, where

$$Y_\pm = \frac{ab - b - c}{2ab} \pm \sqrt{\left(\frac{ab - b - c}{2ab}\right)^2 + \frac{b-1}{ab}}. \tag{11}$$

We note that, at the equilibrium, $X_\pm = 1 - Y_\pm$, and that if $b > 1$ then Y_+ exists for any values of the parameters and belongs to $]0, 1[$. Hence, the parameter b is the basic reproduction number and $b = 1$ is the critical threshold for the existence of the endemic equilibrium. We also note that if $b > 1$, then Y_- becomes strictly negative and, therefore, is not an epidemiologically feasible solution.

Remark 1. There is a second type of substitutions that allow to compute all the equilibria. Being $\tilde{Z} = \tilde{Y}$, one can use the first equation to deduce that

$$\tilde{X} = \frac{1 + c\tilde{Y}}{ab\tilde{Y}^2 + (b + c)\tilde{Y} + 1}. \tag{12}$$

Substituting this quantity in the second equation yields that the equilibria must satisfy the third degree polynomial: $\tilde{Y}(ab\tilde{Y}^2 + (b + c - ab)\tilde{Y} + (1 - b)) = 0$.

This way to obtain the equilibria is particularly useful since in the next section we want to apply the results obtained in [31] associated to the existence of *chains of equilibria*. In fact, we will consider the curve

$$Y \mapsto \left(\frac{1 + cY}{abY^2 + (b + c)Y + 1}, Y, Y\right), \tag{13}$$

and it will be useful that it includes the solution $X = 1$ and $Y = Z = 0$ (i.e., the DFE).

The conditions for the existence of the DFE and the endemic equilibria are summarized in Table 1. It is worth to mention that when $a > c+1$

Table 1
Conditions for the existence of the disease-free equilibrium (DFE) and the endemic equilibria (E_-, E_+). The quantities b_c, Y_- and Y_+ are given in (11) and (14).

$b \in$	$]0, b_c[$	$\{b_c\}$	$]b_c, 1[$	$]1+\infty[$	graphical representation
$a < c+1$	DFE	DFE	DFE	DFE E_+	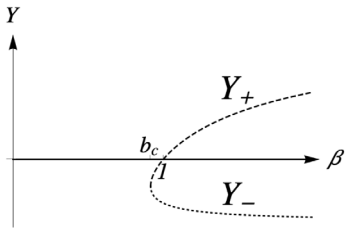
$a > c+1$	DFE	DFE E_+ ‖ E_-	DFE E_- E_+	DFE E_+	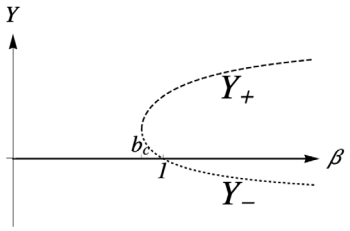

a transcritical *backward bifurcation* takes place at $b = 1$, associated with a saddle-node bifurcation at $b = b_c$, where

$$b_c = \frac{\left(\sqrt{a(c+1)} + \sqrt{a-c}\right)^2}{(a+1)^2}. \tag{14}$$

Backward bifurcation is nowadays a well known feature of some epidemic models [32]. It must be pointed out that it may play a relevant role for disease control and eradication. Indeed, when a backward bifurcation occurs, an endemic equilibria may also exist for values of the basic reproduction number, say R_0, below (but usually close to) the classical threshold $R_0 = 1$. Therefore, in this case it might not be sufficient to reduce the basic reproduction number below the threshold to eliminate the disease.

4. Spectral analysis and simulations

We shortly recall that in the analysis of spectra stability of equilibria one can compute the spectrum of the Jacobian matrix of the vector field at a given equilibrium E. The spectrum gives the spectral type of the equilibrium, that can be classified whenever nondegenerate (see [33]) by means of the symbols $n^3, n^1f^1, n_1^2, n^1f_1, n_1f^1, n_1f_1, n_2^1, n_3$. In this notation n denotes a real eigenvalue (which is called *node*), f indicates a couple of imaginary eigenvalues (which is called *focus*), and the superscript (resp. subscript) indicates the number of positive (resp. negative) real parts of the eigenvalues. A diagram representing the possible type of bifurcations for 3D systems is shown in Fig. 1.

For model (8) the Jacobian matrix of the vector field is:

$$J = \begin{pmatrix} m\left(-1 - bY\dfrac{1+aY}{1+cZ}\right) & -\dfrac{mbX(1+2aY)}{1+cZ} & \dfrac{mcb(1+aY)XY}{(1+cZ)^2} \\ \dfrac{nbY(1+aY)}{1+cZ} & n\left(-1+\dfrac{bX(1+2aY)}{1+cZ}\right) & -\dfrac{ncb(1+aY)XY}{(1+cZ)^2} \\ 0 & 1 & -1 \end{pmatrix} \tag{15}$$

The spectrum of the disease-free equilibrium $DFE = (1, 0, 0)$ is given by $-m$, $n(b-1)$ and -1. It follows that if $b < 1$, then the disease-free equilibrium is stable with spectral type n_3. If $b > 1$, then it is unstable with spectral type n_2^1.

As for the endemic equilibria, as reported in Table 1, if $a < c+1$ the equilibrium E_+ is the only admissible one. It arises with spectral type n_3 and we will show that it evolves first into n_1f_1 and then into n_1f^1. In other words, a *linear Hopf-bifurcation* occurs.

Now consider the curve (13). This curve is well defined and continuous for $Y > 0$ and note that, taking into account of (12), it annihilates the first and third component of the vector field. Therefore, the curve (13) *may* contain some of the equilibria of the vector field in (8) and such equilibria are necessarily ordered by the "parameter of the curve" Y. In [31] it is proven that, along the curve, the determinant of the Jacobian evaluated at each equilibrium of such *chain of equilibria* has alternating sign. In our case, the second component of the vector field in (8) computed along (13) is the function

$$\varphi(Y) = -\frac{Y\left(abY^2 + (b+c-ab)Y + 1 - b\right)}{abY^2 + (b+c)Y + 1}, \tag{16}$$

which annihilates in (and only in) the chain $Y = Y_-$, $Y = 0$, $Y = Y_+$, i.e in the three Y-components of the equilibria E_-, DFE and E_+ of (8). When $b > 1$ the determinant of the Jacobian evaluated at the DFE is positive, and hence the one corresponding to E_+ is negative and it can be of type n_3, n_1f_1, which are stable, or n_1^2, n_1f^1, which are unstable. We will prove that in the parameter space there is a curve of parameters near which a bifurcation from n_1f_1 to n_1f^1 must take place, and we will hence deduce that the system undergoes a linear Hopf bifurcation.

From (9), and $Y_+ = Z_+$, it follows that the Jacobian matrix of the vector field in (8) at E_+ can be written:

$$J(E_+) = \begin{pmatrix} m & 0 & 0 \\ 0 & n & 0 \\ 0 & 0 & 1 \end{pmatrix}\begin{pmatrix} -u-1 & -v-1 & w \\ u & v & -w \\ 0 & 1 & -1 \end{pmatrix},$$

where

$$u = bY_+\frac{1+aY_+}{1+cY_+}, \qquad v = \frac{aY_+}{1+aY_+}, \qquad w = \frac{cY_+}{1+aY_+}.$$

The characteristic polynomial is

$$\chi = -\lambda^3 + \lambda^2(-um+vn-m-1) - \lambda(mu(n+1) - nv(m+1) + wn + m) - mn(u-v+w). \tag{17}$$

Following [33] we recall that the spectral type of an equilibrium of a parameter-dependent vector field is constant with respect to small variations of the parameters. The parameter space is partitioned by three submanifolds defined as zeroes of three algebraic functions that can be obtained through algebraic operations from the characteristic

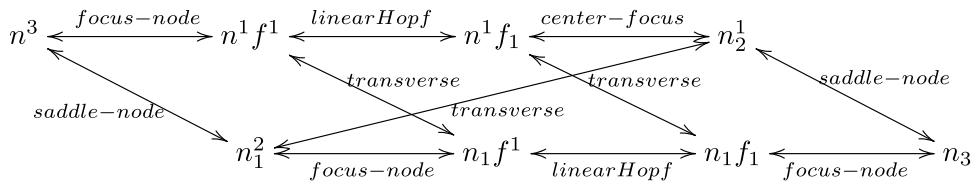

Fig. 1. Diagram representing the type of bifurcations for 3D systems. Here n represents a real eigenvalue, f represents a couple of imaginary eigenvalues. The superscript (resp. subscript) indicates the number of positive (resp. negative) real parts of the eigenvalues.

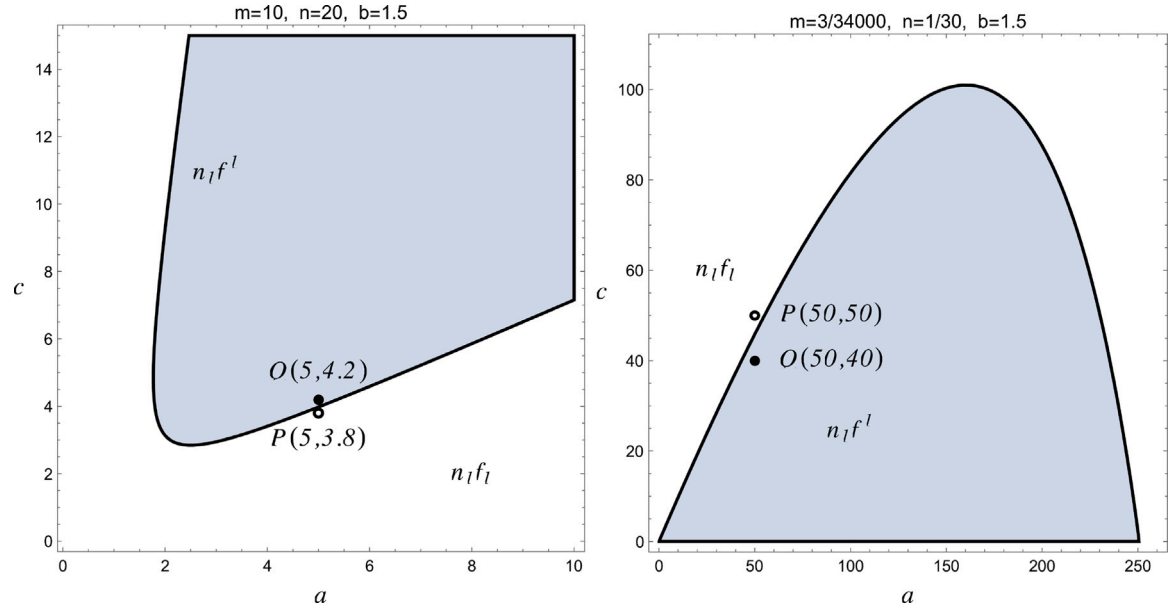

Fig. 2. Curve of linear Hopf bifurcation in the parameter space a, c for the endemic equilibrium E_+ of the prevalence-based model (8). Left panel: the case $(m, n, b) = (10, 20, 1.5)$. Right panel: the case $(m, n, b) = (3/34000, 1/30, 1.5)$. When crossing the curve (which represents the manifold $\mathcal{R}$) a couple of complex conjugate eigenvalues of the vector field linearized at E_+ cross the imaginary axis, and a stable focus becomes an unstable focus. In the shaded region the equilibrium E_+ is unstable, and a limit cycle exists. The black dot corresponds to a choice of parameters a, c for which the equilibrium E_+ is an unstable focus-stable node, the empty dot to a choice for which the equilibrium E_+ is a stable focus-node.

polynomial. The complement of those submanifolds is made by connected open set. In each set the spectral type of the equilibrium is constant. Change of the spectral type between two contiguous open connected components is strictly linked to which of the three submanifolds separates them. In particular, one of such submanifold separates stable focus from unstable focus. That submanifold is the one that we will investigate.

The spectrum of the equilibrium E_+ will change its spectral type when the parameters cross the submanifold $\mathcal{R} = \{(m, n, u, v, w) \mid \rho = 0, \sigma \geq 0\}$, where

$$\rho = m^2(1+u)(1+u+nu-nv)+n(nv-1)(v-w)+m(u+(nv-1)^2+nu(w-(2+n)v)),$$

$$\sigma = m(1 + u + nu - nv) - n(v - w).$$

The conditions $\rho = 0$, $\sigma \geq 0$ are equivalent to require that (17) admits a couple of purely imaginary eigenvalues and can be obtained by imposing $\pm i\mu$, with $\mu \in \mathbf{R}$, as solution of (17) (the algebraic manipulation to get ρ and σ can be found in [33]).

Crossing the submanifold $\mathcal{R}$ will change the spectrum with a Hopf bifurcation.

Note that, in principle, the equilibrium E_+ could change its spectral type also when the parameter values cross the submanifold $\mathcal{Z} = \{(m, n, u, v, w) \mid Z = 0\}$ where

$$Z = u - v + w.$$

since $Z = 0$ implies that the polynomial (17) has a null eigenvalue. However, this can be excluded in our case since we know that the determinant of the Jacobian corresponding to E_+ is always positive.

Recalling that our goal here is to assess the *theoretical* dynamics of the behavioural model (8), we select some baseline parameter values without referring to a specific disease or field case. We take $k = 0.8$ and $\varepsilon = 1/3\, d^{-1}$, two values that were estimated for the first wave of COVID-19 in Italy [7]. In particular, in [7] a weak Erlang memory kernel was used, so that ε assumes the meaning of the inverse of the average time delay of the collected information about the disease prevalence. We also set $b = 1.5$, a basic reproduction number above the threshold $b = 1$, to ensure that the endemic equilibrium E_+ does exist. Furthermore, we consider the two following cases: Set 1 ($m = 10$, $n = 20$), Set 2 ($m = 3/34000$, $n = 1/30$). Note that in Set 2 the value of m correspond to $\mu = 1/34000\, d^{-1}$ (i.e. $\mu = 10.7/1,000 y^{-1}$ as given by the Italian National Institute of Statistics, see [7]).

In Fig. 2 we draw the marginal region $\mathcal{R}$ for the two sets introduced above. It can be seen that in both the cases there is a region in (a, c)-plane (labelled with $n_1 f^1$) in which the endemic equilibrium is an unstable 2D focus together with an stable node and a region (labelled with $n_1 f_1$) in which the endemic equilibrium is a stable 2D focus together with a stable node.

It is this worth to emphasize that disregarding peer-pressure ($a = 0$) or behavioural response to information ($c = 0$), may result in a stable endemic equilibrium (Fig. 2, left panel). This phenomenon takes place only for a restricted ranges of the parameter values of m and n. Indeed, when the values of m and n are very small, sustained oscillations can occur even without behavioural response (Fig. 2, right panel) as it was also observed by Jin et al. [27].

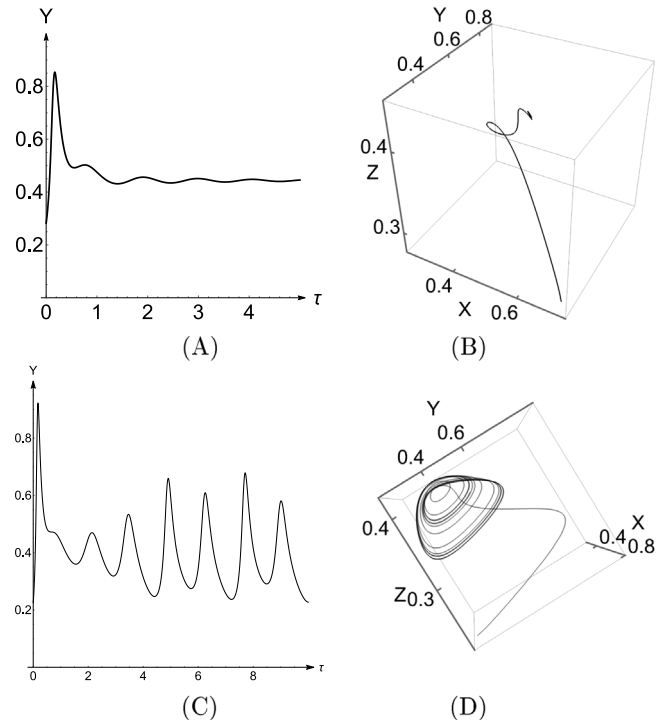

Fig. 3. Numerical simulation of model (8) in the case $m = 10$, $n = 20$. The other values are $k = 0.8$, $\epsilon = 1/3$, $b = 1.5$. The values of a and c correspond to the two points indicated in Fig. 2 left. Panel A and C: temporal dynamics of the nondimensional variable Y representing the infectious population. Panel B and D: orbits in the space XYZ. Plots A and B refer to point P in Fig. 2 left and show convergence to the endemic equilibrium. Panels C and D refer to point Q in Fig. 2 left and show convergence to a limit cycle.

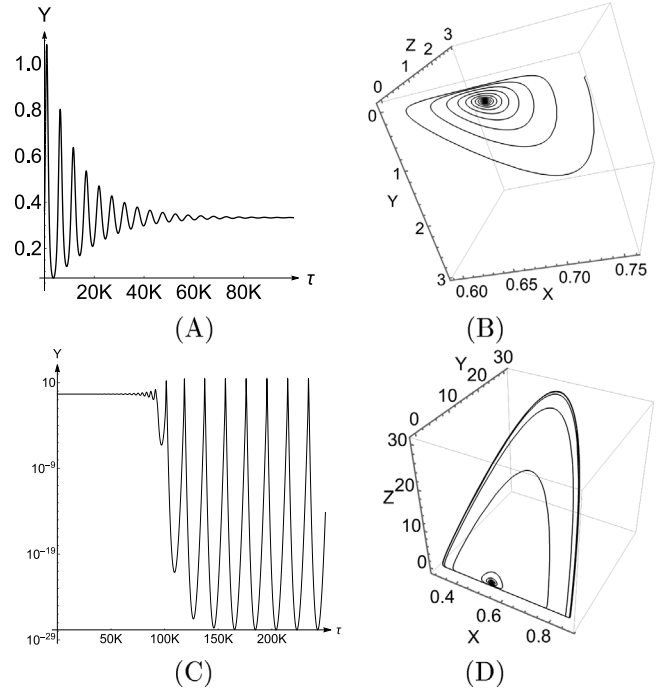

Fig. 4. Numerical simulation of model (8) in the case $m = 3/34000$, $n = 1/30$. The other values are $k = 0.8$, $\epsilon = 1/3$, $b = 1.5$. The values of a and c correspond to the two points indicated in Fig. 2 right. Panel A and C: temporal dynamics of the nondimensional variable Y representing the infectious population (panel C is a logplot, to make the solution more visible). Panel B and D: orbits in the space XYZ. Plots A and B refer to point P in Fig. 2 right and show convergence to the endemic equilibrium. Panels C and D refer to point Q in Fig. 2 right and show convergence to a limit cycle.

In Fig. 3, right panel, we consider values of the parameters a and c in the stability region (the white dot in Fig. 2, left panel) and show the convergence to an equilibrium state. In Fig. 3, left panel, we consider the case of parameters a and c in the instability region (the black dot in Fig. 2, left panel) and show the convergence towards sustained oscillations. In Fig. 4 we get similar dynamics in the case of Set 2. These plots are a strong indication that the Hopf bifurcation is indeed *supercritical*.

5. The incidence-based SIM model with overexposure

In this Section we briefly discuss the case of incidence-based behavioural model, i.e. we replace the message function (5) with

$$g_{inc}(\tau) = h\frac{\beta}{1+\zeta M(\tau)}(1+\alpha I(\tau))S(\tau)I(\tau). \tag{18}$$

Using the linear trick, the model reads

$$\begin{aligned}\dot{S} &= \mu(1-S) - \beta\frac{1+\alpha I}{1+\zeta M}SI\\ \dot{I} &= -\nu I + \beta\frac{1+\alpha I}{1+\zeta M}SI\\ \dot{M} &= \varepsilon\left(h\beta\frac{1+\alpha I}{1+\zeta M}SI - M\right).\end{aligned} \tag{19}$$

The nondimensional form of the vector field can be obtained rescaling time $\tau = \epsilon t$, changing the independent variables and remaining the parameters according to

$$X = S, \quad Y = \frac{\nu}{\mu}I, \quad Z = \frac{1}{h\mu}M, \quad a = \frac{\mu}{\nu}\alpha,$$
$$b = \frac{\beta}{\nu}, \quad c = \mu h\zeta, \quad m = \frac{\mu}{\varepsilon}, \quad n = \frac{\nu}{\varepsilon}.$$

We thus obtain the equations

$$\begin{aligned}X' &= m\left[1 - X - b\frac{1+aY}{1+cZ}XY\right]\\ Y' &= n\left[-Y + b\frac{1+aY}{1+cZ}XY\right]\\ Z' &= b\frac{1+aY}{1+cZ}XY - Z\end{aligned}$$

To determine the equilibria we set the right hand sides of the equations to zero. The third of such equations gives $Z = b(1+aY)/(1+cZ)XY$. Substituting this in the second equation one gets $Z = Y$. This equality makes the second and third equations dependent, and they can be used to obtain $X = (1+cY)/(b+abY)$. After substitution of this quantity, the first equation is positively proportional to the polynomial (10) found in the preceding analysis. Therefore, it follows that the equilibria have the same bifurcation pattern of the equilibria of the incidence-based model.

The disease-free equilibrium has spectrum $-1, -m, and (-1+b)n$. It is hence spectrally stable if $b < 1$ and becomes unstable of type n_2^1 when $b > 1$. When $b > 1$ the determinant of the Jacobian evaluated at the DFE is positive, and hence the one corresponding to E_+ is negative, and it can be of type n_3, $n_1 f_1$, which are stable, or n_1^2, $n_1 f^1$, which are unstable. As in the previous case, we will prove that there is a curve of parameters in the parameter space near which a bifurcation from $n_1 f_1$ to $n_1 f^1$ must take place, and we will hence deduce that the system undergoes a linear Hopf bifurcation.

The endemic equilibrium E_+ of (19) has component

$$Y_+ = \frac{1}{2} - \frac{b+c}{2ab} + \frac{\sqrt{ab((a+2)b-2(c+2))+(b+c)^2}}{2ab}.$$

The linearization of the vector field associated to the system at E_+ has matrix

$$J(E_+) = \begin{pmatrix} m & 0 & 0\\ 0 & n & 0\\ 0 & 0 & 1\end{pmatrix}\begin{pmatrix} -u-1 & -v-1 & w\\ u & v & -w\\ u & v+1 & -w-1\end{pmatrix},$$

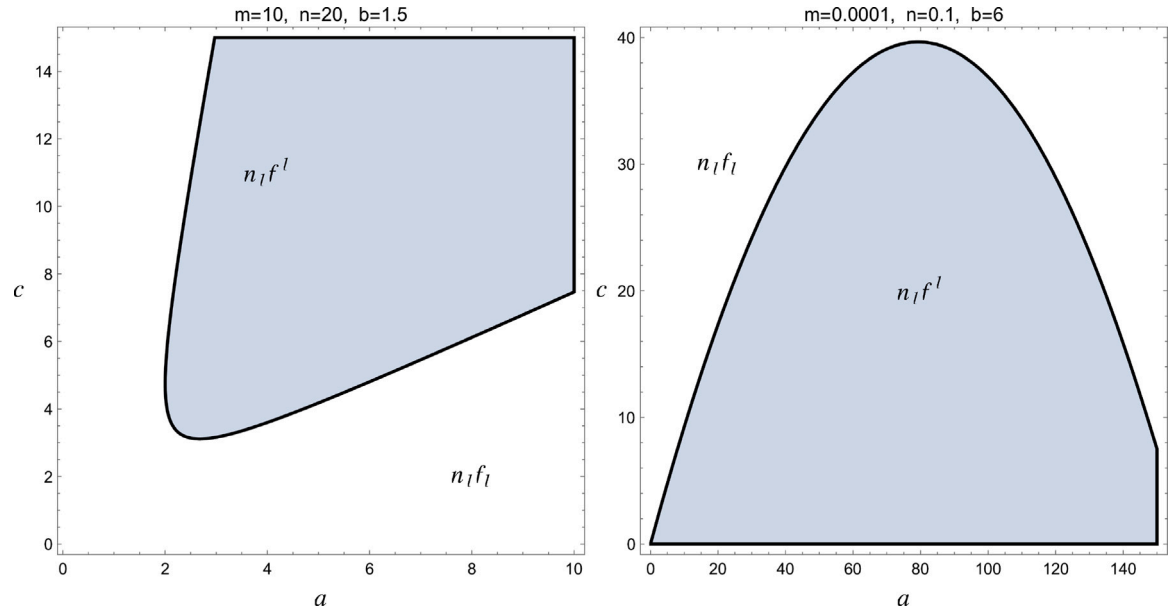

Fig. 5. The two figures show, for different choices of the parameters (m, n, b) the curve of linear Hopf bifurcation in parameter space a, c for the incidence-based model (19). Left panel: $(m, n, b) = (10, 20, 1.5)$. Right panel: $(m, n, b) = (0.0001, 0.1, 6)$. In the shaded region the equilibrium E_+ is unstable, and a limit cycle exists. Across the black curve a couple of complex conjugate eigenvalues of the vector field linearized at E_+ cross the imaginary axis, and a stable focus becomes an unstable focus.

where

$$u = \frac{bY_+(aY_+ + 1)}{cY_+ + 1}, \qquad v = \frac{aY_+}{aY_+ + 1}, \qquad w = \frac{cY_+}{cY_+ + 1}.$$

The characteristic polynomial is

$$-\lambda^3+\lambda^2(-m(u+1)+nv-w-1)+\lambda(mn(v-u)-m(u+w-1)+n(v-w))-mn(u-v+w).$$

The discriminants/resultants can be easily computed, but we do not detail them here (see [33]). A picture of the discriminant locus for this case is similar to that of the prevalence-based model (see Fig. 5) so that similar conclusions can be obtained.

6. Conclusions

In this work we provide a contribution to the analysis of minimal SIR-like behaviour-explicit models, where the force of infection depends on the current and past evolution of the epidemics through the information index [12]. In particular, we focus on the interplay between individuals' behavioural response to the available information and the phenomenon of overexposure that may result from unconscious exposure to contagion. To this aim, we build a SIR-like behavioural model including a contact rate depending on the information index (to represent information-dependent social distancing) and a convex force of infection.

While it is known that when overexposure is not present the human behavioural changes in contact patterns may induce sustained oscillations only when the Erlangian kernel is at least of second order [16, 19], our results show that when overexposure is present, information-dependent social distancing may induce sustained oscillations also in the case of first order Erlangian kernel, i.e. when the memory of the population is exponentially fading. Furthermore, we obtain that when the oscillations are induced by overexposure, the individual's behavioural response to information may stabilize them. These results hold in both the case of prevalence-based and incidence-based social distancing.

Although providing new insights regarding the analysis of minimal behavioural models, like in [19,29] and recently, in [14,16], our work has some limitations. First, the model does not consider pharmaceutical interventions like vaccination. The mutual influence between the decline in prevalence, due to the rise of vaccination coverage, and the consequent decrease in the compliance to social distancing may induce specific phenomena like a switch from a cyclic regime to damped oscillations [20]. Second, considering extrinsic stochastic perturbations could be better represent the evolution of small populations. Finally, field-data are needed to confirm if for realistic sets of parameter values it is possible to have oscillations induced by the simultaneous presence of behavioural response to information and overexposure. However, parametrization of behavioural models on real cases are, in principle, possible [7]. These issues will be matter of future work.

Declaration of competing interest

The authors declare that they have no known competing financial interests or personal relationships that could have appeared to influence the work reported in this paper.

Data availability

No data was used for the research described in the article.

Acknowledgements

The authors thank Alberto d'Onofrio (University of Trieste) for his valuable suggestions and discussions.

This work has been performed under the auspices of the Italian National Group for Mathematical Physics (GNFM) of the National Institute for Advanced Mathematics (INdAM).

B.B. acknowledges EU funding within the NextGenerationEU—MUR PNRR Extended Partnership initiative on Emerging Infectious Diseases (Project no. PE00000007, INF-ACT) and PRIN 2020 project (No. 2020JLWP23) "Integrated Mathematical Approaches to Socio–Epidemiological Dynamics".

A.G. acknowledges PRIN 2017 project (No. 2017YBKNCE) and grant PIA.CE.RI. 53722122146 of the University of Catania, Italy.

Appendix. Positive invariance and boundedness

We prove that the solution of system (8) are positive and bounded by showing that a prism in the positive octant is invariant. Let us

consider the prism with the following edges: $X = 0$, $Y = 0$, $Z = 0$, $X + m/nY = 1$ (a triangle in X, Y plane), and $Z = n/m$. Denote by $\mathbf{f}$ the vector field of (8) and by $\mathbf{n}_i$, $i = 1, \dots, 5$, the outgoing normal to the ith edge of the prism. On the first edge ($X = 0$) one has $\mathbf{n}_1 = (-1, 0, 0)$ and $\langle \mathbf{f}, \mathbf{n}_1 \rangle = -m < 0$, so that $X \geq 0$. On the second edge ($Y = 0$) one has $\mathbf{n}_2 = (0, -1, 0)$ and $\langle \mathbf{f}, \mathbf{n}_2 \rangle = 0$. However, when $Y = 0$ the solution of (8) converges globally to $X = 1$, $Z = 0$, for any initial data in the plane $Y = 0$ which is, therefore, invariant and $Y \geq 0$. On the third edge ($Z = 0$) one has $\mathbf{n}_3 = (0, 0, -1)$ and $\langle \mathbf{f}, \mathbf{n}_3 \rangle = -Y \leq 0$, so that $Z \geq 0$. On the fourth edge ($X + m/nY = 1$) one has $\mathbf{n}_4 = (1, m/n, 0)$ and $\langle \mathbf{f}, \mathbf{n}_4 \rangle = (m/n)(m - n)Y < 0$ being $m < n$. Finally, on the fifth edge ($Z = n/m$) one has $\mathbf{n}_5 = (0, 0, 1)$ and $\langle \mathbf{f}, \mathbf{n}_5 \rangle = Y - (n/m) \leq 0$ being $X + m/nY \leq 1$.

References

[1] Flaxman S, Mishra S, Gandy A, Unwin HJT, Mellan TA, Coupland H, et al. Estimating the effects of non–pharmaceutical interventions on COVID–19 in Europe. Nature 2020;584:257–61.

[2] Ngonghala CN, Iboi E, Eikenberry S, Scotch M, MacIntyre CR, Bonds MH, et al. Mathematical assessment of the impact of non–pharmaceutical interventions on curtailing the 2019 novel coronavirus. Math Biosci 2020;325:108364.

[3] Parolini N, Dedè L, Antonietti PF, Ardenghi G, Manzoni A, Miglio E, et al. SUIHTER: a new mathematical model for COVID-19. Application to the analysis of the second epidemic outbreak in Italy. Proc R Soc A Math Phys Eng Sci 2021;477(2253):20210027.

[4] Poletti P, Ajelli M, Merler S. Risk perception and effectiveness of uncoordinated behavioral responses in an emerging epidemic. Math Biosci 2012;238(2):80–9.

[5] Brauer F, Van den Driessche P, Wu J. Mathematical epidemiology, vol. 1945. Springer; 2008.

[6] Martcheva M. An introduction to mathematical epidemiology, vol. 61. Springer; 2015.

[7] Buonomo B, Della Marca R. Effects of information–induced behavioural changes during the COVID–19 lockdowns: the case of Italy. R Soc Open Sci 2020;7(10):201635.

[8] Della Rossa F, Salzano D, Di Meglio A, De Lellis F, Coraggio M, Calabrese C, et al. A network model of Italy shows that intermittent regional strategies can alleviate the COVID-19 epidemic. Nature Commun 2020;11(1):1–9.

[9] Gatto M, Bertuzzo E, Mari L, Miccoli S, Carraro L, Casagrandi R, et al. Spread and dynamics of the COVID–19 epidemic in Italy: Effects of emergency containment measures. Proc Natl Acad Sci 2020;117(19):10484–91.

[10] Giordano G, Colaneri M, Di Filippo A, Blanchini F, Bolzern P, De Nicolao G, et al. Modeling vaccination rollouts, SARS-CoV-2 variants and the requirement for non-pharmaceutical interventions in Italy. Nat Med 2021;27(6):993–8.

[11] Manfredi P, d'Onofrio A, editors. Modeling the interplay between human behavior and the spread of infectious diseases. Springer Science & Business Media; 2013.

[12] Wang Z, Bauch CT, Bhattacharyya S, d'Onofrio A, Manfredi P, Perc M, et al. Statistical physics of vaccination. Phys Rep 2016;664:1–113.

[13] Capasso V, Serio G. A generalization of the Kermack–McKendrick deterministic epidemic model. Math Biosci 1978;42(1):43–61.

[14] d'Onofrio A, Manfredi P. The interplay between voluntary vaccination and reduction of risky behavior: a general behavior-implicit SIR model for vaccine preventable infections. In: Aguiar M, et al., editors. Current trends in dynamical systems in biology and natural sciences. Springer; 2020, p. 185–203.

[15] d'Onofrio A. Vaccination policies and nonlinear force of infection: generalization of an observation by Alexander and Moghadas (2004). Appl Math Comput 2005;168(1):613–22.

[16] d'Onofrio A, Manfredi P. Behavioral SIR models with incidence-based social-distancing. Chaos Solitons Fractals 2022;159:112072.

[17] López-Cruz R. Global stability of an SAIRD epidemiological model with negative feedback. Adv Continuous Discret Model 2022;2022(1):1–13.

[18] Zhu L, Zhou X, Li Y, Zhu Y. Stability and bifurcation analysis on a delayed epidemic model with information-dependent vaccination. Phys Scr 2019;94(12):125202.

[19] d'Onofrio A, Manfredi P. Information-related changes in contact patterns may trigger oscillations in the endemic prevalence of infectious diseases. J Theoret Biol 2009;256(3):473–8.

[20] Buonomo B, Della Marca R, Sharbayta SS. A behavioral change model to assess vaccination-indiced relaxation of social distancing during an epidemic. J Biol Systems 2022;30(01):1–25.

[21] van den Driessche P, Watmough J. A simple SIS epidemic model with a backward bifurcation. J Math Biol 2000;40(6):525–40.

[22] Lacitignola D, Saccomandi G. Managing awareness can avoid hysteresis in disease spread: An application to coronavirus COVID-19. Chaos Solitons Fractals 2021;144:110739.

[23] Lacitignola D, Diele F. Using awareness to Z-control a SEIR model with overexposure: Insights on Covid-19 pandemic. Chaos Solitons Fractals 2021;150:111063.

[24] Santor DA, Messervey D, Kusumakar V. Measuring peer pressure, popularity, and conformity in adolescent boys and girls: Predicting school performance, sexual attitudes, and substance abuse. J Youth Adolesc. 2000;29(2):163–82.

[25] Buonomo B, Lacitignola D. Modeling peer influence effects on the spread of high–risk alcohol consumption behavior. Ric Mat 2014;63(1):101–17.

[26] Mushanyu J, Nyabadza F, Muchatibaya G, Stewart A. On the role of imitation on adolescence methamphetamine abuse dynamics. Acta Biotheor 2017;65(1):37–61.

[27] Jin Y, Wang W, Xiao S. An SIRS model with a nonlinear incidence rate. Chaos Solitons Fractals 2007;34(5):1482–97.

[28] Van den Driessche P, Watmough J. Epidemic solutions and endemic catastrophes. In: Ruan S, Wolkowicz GS, Wu J, editors. Dynamical systems and their applications in biology. Fields Institute Communications; 2003, p. 185–203.

[29] Buonomo B, d'Onofrio A, Lacitignola D. Global stability of an SIR epidemic model with information dependent vaccination. Math Biosci 2008;216(1):9–16.

[30] MacDonald N. Biological delay systems: linear stability theory. Cambridge University Press; 2008.

[31] Giacobbe A, Mulone G. Stability of ordered equilibria. J Math Anal Appl 2018;462(2):1298–308.

[32] Gumel AB. Causes of backward bifurcations in some epidemiological models. J Math Anal Appl 2012;395(1):355–65.

[33] Giacobbe A. An algebro-geometric classification of spectral types of equilibria. 2020, arXiv preprint arXiv:2012.03024.